



OPEN Highly oriented pyrolytic graphite chemical bonding structure after gallium implantation

T. A. O. Jafer¹, H. A. A. Abdelbagi², A. Sulyok³, G. Z. Radnóczy³, K. Tőkési⁴✉ & J. B. Malherbe¹

Highly oriented pyrolytic graphite (HOPG) structural changes caused by gallium (Ga) implantation at room temperature were investigated. Ga ions were implanted into HOPG at different energies (10, 20, and 30 keV) and fluences (ranging from 2×10^{15} to 5×10^{16} Ga⁺/cm²). To monitor structural changes in the samples post-implantation, Raman spectroscopy was employed. The Raman spectra of the pristine HOPG sample displayed low-intensity D peaks at 1359 cm⁻¹ and high-intensity G peaks at 1582 cm⁻¹. After implantation with 10 keV at a fluence of 5×10^{16} Ga⁺/cm², a decrease in G peak intensity was observed, accompanied by an increase in its full width at half maximum (FWHM), indicating defect formation in the HOPG structure. In contrast, implantation with 30 keV at the same fluence (5×10^{16} Ga⁺/cm²) resulted in the merging of the D and G peaks into a broad peak, signifying the amorphization of HOPG. These results confirm that ion energy plays a significant role in the amorphization of HOPG. Furthermore, implantation with 20 keV Ga ions at fluences $\leq 2 \times 10^{16}$ Ga⁺/cm² introduced some defects in the HOPG structure, while higher fluences ($\geq 4 \times 10^{16}$ Ga⁺/cm²) led to complete amorphization. After comparing the Raman results with the threshold displacement per atom (dpa) values calculated using the SRIM (Stopping and Range of Ions in Matter) software, it is evident that the HOPG used in this study required a very high dpa (exceeding 35 dpa) for complete amorphization, significantly exceeding the previously suggested range of 0.2 dpa to 3 dpa. The findings of this study align with very few prior results, where no amorphization was observed above 3 dpa. However, further research and testing are necessary to quantify the dpa required for HOPG amorphization.

Keywords Raman spectroscopy, HOPG, Gallium implantation, Amorphization

Highly oriented pyrolytic graphite (HOPG) is a synthetic carbon material renowned for its unique structural and functional properties, derived from its highly ordered polycrystalline arrangement of graphene sheets¹. This material is characterized by domain sizes typically ranging from 1 to 10 μm along the main plane and less than 0.1 μm perpendicular to it. The structural features confer HOPG with exceptional thermal conductivity, high electrical conductivity, and superior mechanical stability, making it a material of significant interest in both fundamental research and practical applications². In particular, HOPG has found extensive use in nuclear environments, where its properties are leveraged in neutron moderators, beamline components, and radiation detectors^{3–6}.

The performance of HOPG in high-radiation environments, such as those encountered in fission reactors and spallation neutron sources, is critically dependent on its ability to withstand intense neutron and ion irradiation. Under such conditions, HOPG experiences atomic displacements, structural disorder, and a progressive degradation of its functional properties^{4,7}. A key metric for assessing the radiation resistance of HOPG is the displacement per atom (dpa) threshold, which represents the radiation dose required to induce significant lattice damage and potentially transform the material into an amorphous state⁸. Quantitating this threshold is crucial for predicting the material's behavior and ensuring its long-term stability in demanding applications.

The structural changes in HOPG after ion implantation at different temperatures have been extensively studied^{9–20}. Most studies agree that the threshold for amorphizing HOPG after ion bombardment at room temperature (RT), irrespective of the ions implanted, is approximately between 0.2 and 3 dpa^{9–15}. However,

¹Physics Department, University of Pretoria, Hatfield, Pretoria, South Africa. ²Physics Department, University of Zululand, KwaDlangezwa, Richards Bay 3886, South Africa. ³HUN-REN Centre for Energy Research, Institute of Technical Physics and Materials Science, Budapest, Hungary. ⁴HUN-REN Institute for Nuclear Research (ATOMKI), Debrecen, Hungary. ✉email: tokesi@atomki.hu

conflicting results have been reported in HOPG samples implanted at RT, with some studies observing only some defects (without amorphization) even at high damage levels (> 3 dpa)^{17,18}. Melinon et al.¹⁹ reported total amorphization above 10 dpa. These discrepancies in the minimum dpa required to amorphize HOPG after ions bombardment at RT highlight the need for further research to resolve inconsistencies in the literature.

This study investigates the structural effects of gallium ions implantation on HOPG. Ga ions were implanted into HOPG at room temperature with energies of 10, 20 and 30 keV, and at fluences ranging from 2×10^{15} ions/cm² to 5×10^{16} ions/cm². Different energies and fluences were used to obtain the threshold dpa for HOPG amorphization. Visible-Raman spectroscopy was used to monitor structural changes due to different implantation energies and fluences.

Due to differences in implantation fluence, the D and G characteristic bands in the Raman spectra exhibited significant changes, such as merging into a broad band. Consequently, different fitting functions were employed to analyze the Raman spectra, as described in the experimental section.

Experimental procedure

In this study, HOPG samples from *SPI Supplies* were used. The as-received samples were implanted with Ga ions using a Scios 2 (ThermoScientific) equipment. Though, this equipment was designed for fine ion beam (FIB) operations exploiting its well-focused Ga beam, it can be used for our purpose of implantation adjusting a highly defocused beam. This defocused beam was scanned over $200\mu\text{m} \times 200\mu\text{m}$ area (see Fig. 1) to provide a large and evenly radiated surface for further investigations.

The sample was implanted at a normal angle of incidence separately with Ga ions at 10, 20 and 30 keV at room temperature and fluences of 2×10^{15} , 5×10^{15} , 1×10^{16} , 2×10^{16} , 4×10^{16} and 5×10^{16} ions/cm² to 5×10^{16} ions/cm². The flux was kept at 1×10^{12} Ga⁺ cm⁻² s⁻¹ in order to avoid heating the substrate, which could lead to additional structural changes^{21,22}. The implanted areas can be well identified by a secondary electron image as shown in Fig. 1.

The effect of Ga implantation (at different energies and fluences) on the microstructure of HOPG substrates was monitored with WITec Alpha 300 confocal Raman spectroscopy. At a laser wavelength of 532 nm, Raman spectra were acquired with a $100 \times 0.9\text{NA}$ objective lens and a 5mW laser excitation. By dividing the wavelength by the extinction coefficient in the following equation, $z = \lambda / 4\pi k$ ²³, the penetration depth of the 532 nm laser was calculated, which is 50 nm. Raman spectra were collected from three different points within each implanted area, and their average values were plotted in the results section. To analyse the HOPG Raman spectra, the baseline of the spectral lines was first corrected by linear background correction. To obtain the full width at half maximum (FWHM) and peak positions, both Gaussian and Breit–Wigner–Fano (BWF) functions were used to fit the spectra using the OriginLab software program²⁴. Errors in the FWHM values were estimated from combining

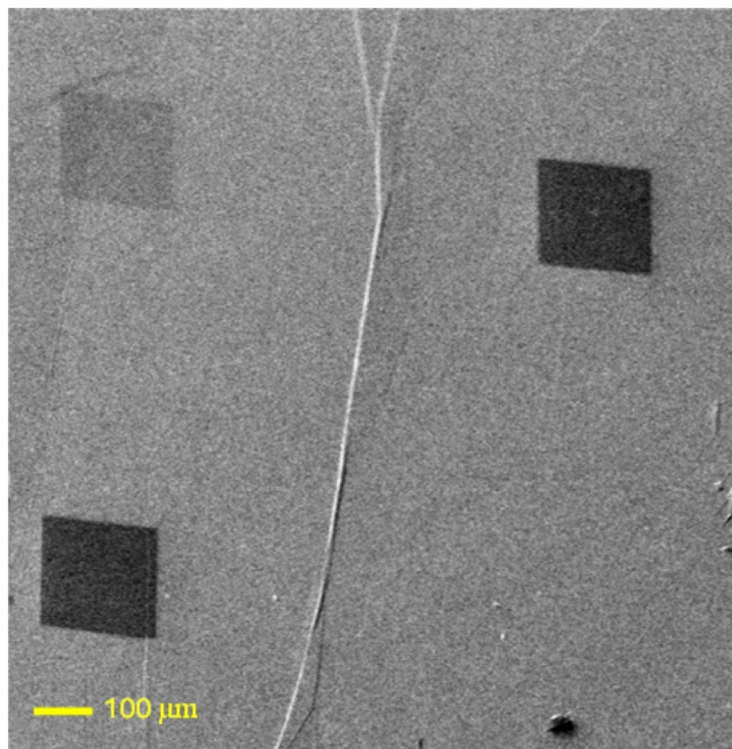


Fig. 1. Secondary electron image taken on HOPG surface after Ga implantation. The implanted areas have square shape. The image show parallelogram shapes because of projected angle of the image taken. The different shades are due to different implanted fluences with the higher fluences being darker.

statistical and systematic errors and found to be less than 5.5 cm^{-1} , and should not change the obtained results significantly.

SRIM simulations

SRIM (Stopping Range of Ions in Matter)²⁵ simulations were carried out to estimate radiation damage as well as the dpa caused to HOPG substrates by Ga ions implanted at different energies and fluences—see Fig. 2. Radiation damage is typically measured by estimating the average number of atoms that are displaced from their lattice sites during implantation (dpa). The depth profile of Ga ions implanted in HOPG was simulated using SRIM's full cascade mode. Due to the statistical nature of collisions between energetic impinging ions with substrate atoms, Ga depth distribution in HOPG have a Gaussian shape²¹. In this simulation, the HOPG carbon density was assumed to be $2.25 \text{ g/cm}^3 \sim 11.3 \times 10^{22} \text{ atoms/cm}^3$ and a carbon displacement energy of 20 eV was used. Figure 2 shows different damage levels (in displacement per atom (dpa)) in HOPG after implantation at varying energies and fluences according to our SRIM simulations. However, the maximum damage level in all samples is significantly higher than the reported critical displacement per atom value of 0.2 dpa required to amorphize HOPG^{9–15}. Based on the simulation of Ga in HOPG, the amorphization thickness in the HOPG substrate varies with ion energy and fluence—see Fig. 2 and Table 1. The thickness of the amorphized layer was determined from the dpa profile (see Fig. 2), with the depth corresponding to 0.2 dpa indicating the layer's thickness.

Results and discussion

Figure 3 shows the Raman spectra of pristine HOPG samples before and after implantation with Ga ions at 10 and 30 keV and at different fluences. Raman spectra of pristine HOPG show the D and G characteristic bands at 1354 cm^{-1} and 1581 cm^{-1} , respectively. It is known that the D peak is originated by disordered sp^3 bonds, whereas the G peak is caused by sp^2 vibrations of graphite²⁶. From these two peaks, the structure of HOPG was predominantly graphite, although some amorphous carbon was also observed. Moreover, implantation with 10 keV Ga ions at $5 \times 10^{15} \text{ cm}^{-2}$ increased the intensity of the D peak accompanied by a decrease in the intensity of the G peak. However, the G peak intensity is still higher than D peak intensity. It is clear from the results that implantation converted some graphitic crystallites in the HOPG sample to amorphous carbon^{26,27}, but the sample still contains some graphitic characteristics. Implantation with 10 keV at higher fluence ($5 \times 10^{16} \text{ cm}^{-2}$) caused further decrease in G peak, accompanied by more broadening in the D peaks (will be discussed later in Table 2) which indicates that higher fluence converted more graphitic crystallites into amorphous carbon²⁶. Comparing these results with the dpa values shown in Fig. 1a, it is clear that implantation with 10 keV Ga ions at high fluence will create a thin amorphous layer with a thickness of 23 nm at the surface (at 0.2 dpa [9–12]). Thus, by comparing again the thickness of the amorphous layer with the penetration depth of the Raman laser mentioned above (about 50 nm), the G peaks in the Raman spectrum of samples implanted with 10 keV Ga ions (at $5 \times 10^{16} \text{ cm}^{-2}$) may be from the region below the implanted layer.

On the other hand, implantation at 30 keV at a fluence of $5 \times 10^{15} \text{ cm}^{-2}$ increased the intensity of the D peak significantly to the same intensity of its G peak which reduced as well after implantation. In HOPG samples, the intensity ratio between D and G bands, i.e. (ID/IG ratio), can help estimate defects²⁸. A higher ratio between D and G bands indicates more defects in the HOPG structure²⁸. As calculated from Fig. 3, the intensity ratio in the samples implanted with 30 keV at a fluence of $5 \times 10^{15} \text{ cm}^{-2}$ is equal to 1. However, this ratio was 0.1 in pristine HOPG, which increased to 0.60 and 0.62 in the samples implanted with 10 keV at fluences of $5 \times 10^{15} \text{ cm}^{-2}$ and $5 \times 10^{16} \text{ cm}^{-2}$, respectively. These results indicate that increasing the ions' energy increases the chance of creating highly defected graphite crystals in HOPG. Electronic stopping power must also be considered at energies higher than the one used in this study. Despite this, the D and G peaks are still present after implantation at 30 keV at a fluence of $5 \times 10^{15} \text{ cm}^{-2}$, which indicates that the implanted area is not yet totally amorphous. However, implantation with 30 keV and at higher fluence ($5 \times 10^{16} \text{ cm}^{-2}$) caused the D and G peaks to merge into a single broadband, indicating amorphization of all graphitic crystallites in the implanted region of the HOPG sample^{26,27}. It is also possible that the difference in Raman spectra between samples implanted with 30 keV at different fluences is related to the thickness of the amorphous layer (implantation at the high fluence created a thicker layer (i.e., 52 nm) that was close to the theoretically calculated penetration depth of the Raman laser) created within the HOPG material, as shown in Fig. 1c and Table 1.

Table 2 shows the FWHM of the D and G peaks of the acquired spectra of the HOPG samples before and after implantation with 10 and 30 keV Ga ions at fluences of 5×10^{15} and $5 \times 10^{16} \text{ cm}^{-2}$. From Table 2, the FWHM value of the G peak increased from 20 cm^{-1} (pristine HOPG) to 42 and 78 cm^{-1} after implantation with 10 keV at fluences of 5×10^{15} and $5 \times 10^{16} \text{ cm}^{-2}$, respectively. This broadening is due to the introduction of disorder (point defects) within the substrate structure^{21,22,26,27}. A significant broadening in the FWHM of the G peak was observed after implantation at 30 keV, which indicate more disorder in the HOPG structure. This agrees with the results in Fig. 3, where implantation under these conditions (30 keV, at $5 \times 10^{16} \text{ cm}^{-2}$) caused the D and G peaks to merge into one broadband, indicating amorphization of HOPG. Moreover, the broadening in the G peak after implantation with 30 keV at $5 \times 10^{16} \text{ cm}^{-2}$, was accompanied by a significant broadening in the D peak, confirming that the implanted layer of HOPG became amorphized.

Figure 4 shows the Raman spectra of pristine HOPG samples before and after implantation with 20 keV Ga ions at different fluences. This experiment was done to gain more understanding of the effect of ion fluences on defects generation behaviour in HOPG. Implantation with 20 keV Ga ions at $2 \times 10^{15} \text{ cm}^{-2}$ and $1 \times 10^{16} \text{ cm}^{-2}$ decreased the intensity of the G peaks, which indicate formation of disorder in the HOPG structure. In addition, the G peaks intensities are still higher than the D peaks intensities after implantation at these fluences. However, implantation at higher fluence (i.e., $2 \times 10^{16} \text{ cm}^{-2}$) caused the D and G peaks to have the same intensities. As mentioned previously in Fig. 3, the higher intensity ratio of the D and G bands indicate the presence of a

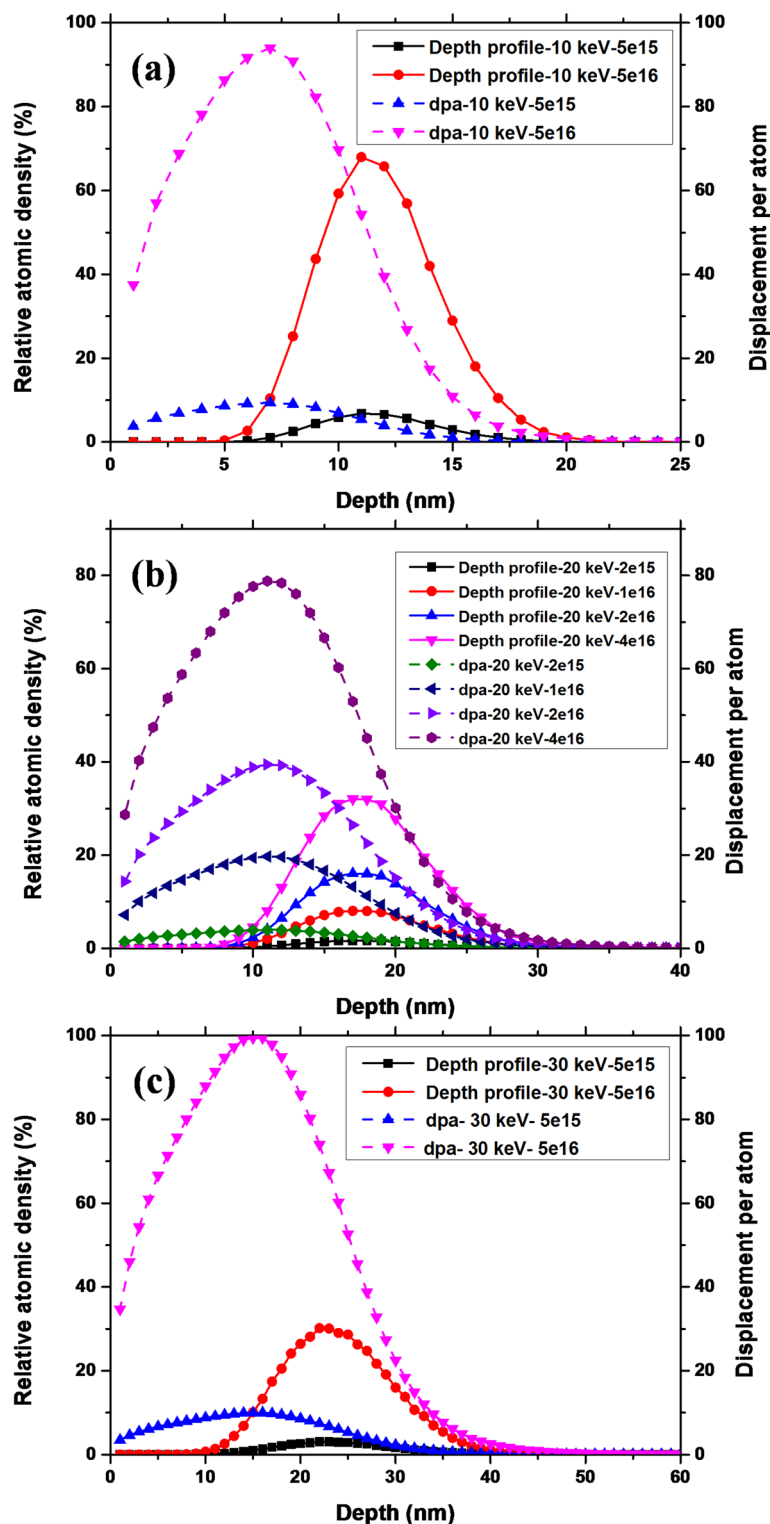


Fig. 2. SRIM depth profiles (in RAD—relative atomic density) of (a) 10 keV (b) 20 keV and (c) 30 keV Ga ions implanted in HOPG at room temperature and different fluences. The damage in dpa is also shown using these ions fluences mentioned in the figure.

highly defective structure of HOPG. From Fig. 4, samples implanted at $2 \times 10^{16} \text{ cm}^{-2}$ have an intensity ratio equal to 1, while in samples implanted at $2 \times 10^{15} \text{ cm}^{-2}$ and $1 \times 10^{16} \text{ cm}^{-2}$ the intensity ratio is equal to 0.4 and 0.62, respectively. This indicates that samples implanted at $2 \times 10^{16} \text{ cm}^{-2}$ have more defects in HOPG structure compared to implanted samples at $2 \times 10^{15} \text{ cm}^{-2}$ and $1 \times 10^{16} \text{ cm}^{-2}$. Moreover, after implantation at $4 \times 10^{16} \text{ cm}^{-2}$, the D and G peaks merged into one broadband, indicating HOPG amorphization at this fluence. Moreover, the

| Ion's energies and fluences | | Thickness of the amorphized layer |
|-----------------------------|------------------------------------|-----------------------------------|
| 10 keV | $5 \times 10^{15} \text{ cm}^{-2}$ | 18 nm |
| | $5 \times 10^{16} \text{ cm}^{-2}$ | 23 nm |
| 20 keV | $2 \times 10^{15} \text{ cm}^{-2}$ | 27 nm |
| | $1 \times 10^{16} \text{ cm}^{-2}$ | 32 nm |
| | $2 \times 10^{16} \text{ cm}^{-2}$ | 35 nm |
| | $4 \times 10^{16} \text{ cm}^{-2}$ | 37.5 nm |
| 30 keV | $5 \times 10^{15} \text{ cm}^{-2}$ | 41 nm |
| | $5 \times 10^{16} \text{ cm}^{-2}$ | 52 nm |

Table 1. The change in the thickness of the amorphized layer in HOPG as a function of ion energies and fluences as predicted by SRIM.

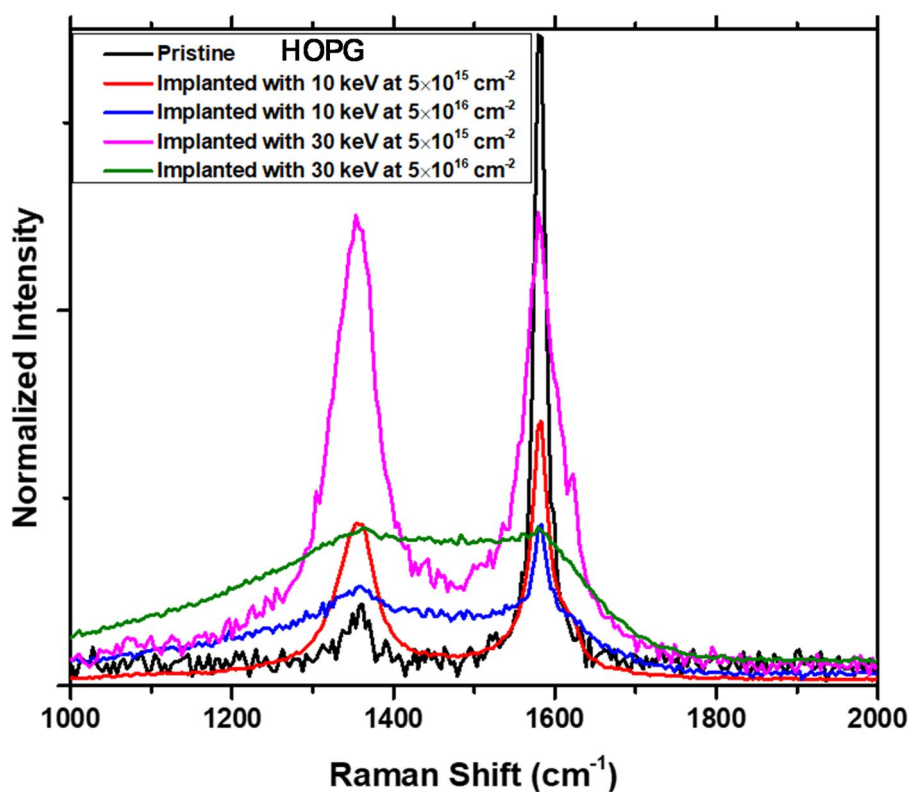


Fig. 3. Raman spectra of pristine HOPG before and after implantation with Ga ions at 10 and 30 keV at different fluences (i.e., 5×10^{15} and $5 \times 10^{16} \text{ cm}^{-2}$).

| Sample | The FWHM of | |
|--|-------------------------------|--------------------------------|
| | D peak | G peak |
| Pristine HOPG | $42.5 \pm 2 \text{ cm}^{-1}$ | $20.2 \pm 1.5 \text{ cm}^{-1}$ |
| 10 keV Ga ions at $5 \times 10^{15} \text{ cm}^{-2}$ | $65 \pm 2.9 \text{ cm}^{-1}$ | $42 \pm 2.7 \text{ cm}^{-1}$ |
| 10 keV Ga ions at $5 \times 10^{16} \text{ cm}^{-2}$ | $87 \pm 3 \text{ cm}^{-1}$ | $78 \pm 5 \text{ cm}^{-1}$ |
| 30 keV Ga ions at $5 \times 10^{15} \text{ cm}^{-2}$ | $82 \pm 4.2 \text{ cm}^{-1}$ | $76 \pm 4.5 \text{ cm}^{-1}$ |
| 30 keV Ga ions at $5 \times 10^{16} \text{ cm}^{-2}$ | $282 \pm 4.9 \text{ cm}^{-1}$ | $140 \pm 5.5 \text{ cm}^{-1}$ |

Table 2. The effect of Ga ion bombardment at 10 and 30 keV and at different fluences on the FWHM values of the D and G peaks of HOPG acquired after fitting the spectra with the BWF function. Errors in the measured values were also included.

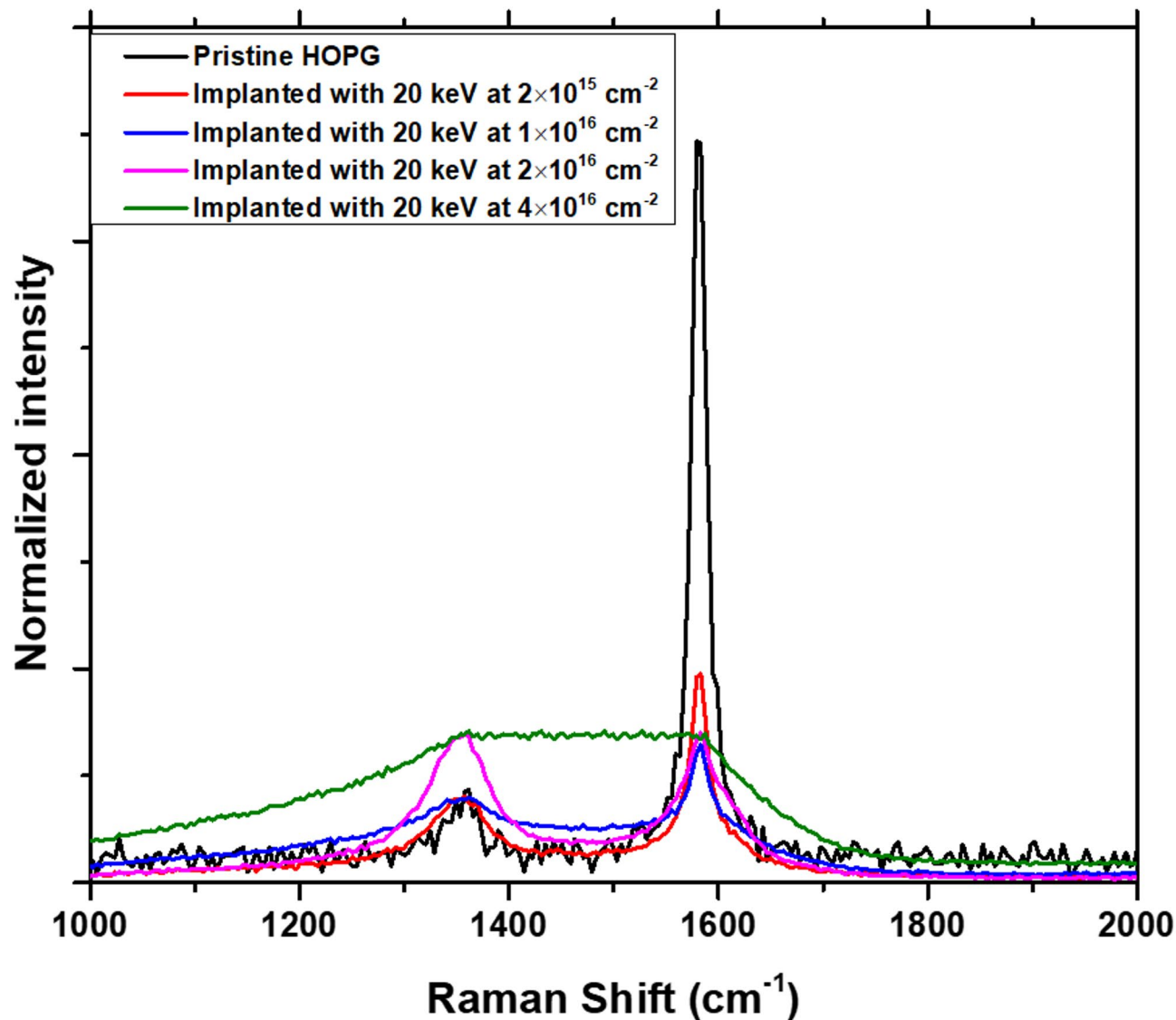


Fig. 4. Raman spectra of pristine HOPG before and after implantation with 20 keV Ga ions at different fluences of $2 \times 10^{15} \text{ cm}^{-2}$, $1 \times 10^{16} \text{ cm}^{-2}$, $2 \times 10^{16} \text{ cm}^{-2}$ and $4 \times 10^{16} \text{ cm}^{-2}$.

FWHM of the pristine HOPG was increased from $20.2 \pm 4 \text{ cm}^{-1}$ to 29.7 ± 4 , 65.4 ± 4 , 87.8 ± 4 and $137 \pm 4 \text{ cm}^{-1}$ after implanting 20 keV Ga ions at $2 \times 10^{15} \text{ cm}^{-2}$, $1 \times 10^{16} \text{ cm}^{-2}$, $2 \times 10^{16} \text{ cm}^{-2}$ and $4 \times 10^{16} \text{ cm}^{-2}$, respectively. These results showed that increasing the ions fluence increases the FWHM of the G peaks in HOPG samples, indicating more defects in HOPG at higher ions fluence ($4 \times 10^{16} \text{ cm}^{-2}$) where amorphization was observed (D and G peaks merged into a broad peak). Comparing our Raman results (in Fig. 4) with the displacement per atom distribution (dpa) in HOPG caused by Ga ions obtained from SRIM simulations (see Fig. 1 (b)), the threshold dpa to amorphize the HOPG samples used in this study can be estimated.

Previous studies suggested that a dpa between 0.2 and 3 dpa is required to amorphize HOPG^{9–15}. However, comparing Figs. 1 and 4, the amorphization of HOPG started at a dpa higher than 35 dpa. The amorphization of HOPG used in this study differs from that reported in earlier studies, likely because of differences in the initial structural quality of the HOPG samples or the specific type of ions used for implantation. For example, if He and Ga ions introduce the same amount of dpa in the substrate, the bombarded ions can behave differently within the HOPG matrix causing discrepancies in the real amount of defects in He and Ga irradiated samples. He ions were found to form bubbles within the HOPG matrix accompanied by blister formation on the surface²⁹, while Ga ions were found to form metallic clusters within the HOPG matrix³⁰. The formation of He bubbles in one sample and Ga clusters in another sample (after the implantation process) could result in differences in the degree of structural disruption of HOPG even if Ga and He ions were implanted at the same dpa levels. Moreover, the HOPG samples used in this study appear to have a highly ordered structure that requires a higher dpa to amorphize it. Using a scanning tunnelling microscope (STM), the HOPG obtained from SPI Supplies (shown at <https://www.2spi.com/catalog/documents/Tech-Note-HOPG.pdf>) was observed to have a perfect crystalline structure. Similar results were observed in a previous study¹⁹, where HOPG exhibited a highly ordered structure

at a dpa < 10 , while a complete amorphization was observed at a dpa higher than 10 dpa. Therefore, the threshold dpa to amorphize the HOPG samples may be highly dependent on the initial structure of the pristine samples.

Conclusion

Raman spectroscopy was employed in this study to investigate the structural changes in highly ordered pyrolytic graphite (HOPG) following gallium implantation at various energies (10, 20, and 30 keV) and fluences (2×10^{15} , 5×10^{15} , 1×10^{16} , 2×10^{16} , 4×10^{16} , and 5×10^{16} cm $^{-2}$). The implantation was conducted at room temperature. SRIM simulations revealed that the damage introduced into the HOPG substrate after implantation significantly exceeds the critical displacement per atom value of 0.2 dpa required to amorphize HOPG. This indicates that all samples implanted at fluences of $\geq 2 \times 10^{15}$ cm $^{-2}$ and above have formed an amorphous layer, with thickness varying according to ion energy and fluence.

However, Raman spectra indicated that only the samples implanted with 20 keV at 4×10^{16} cm $^{-2}$ and 30 keV at 5×10^{16} cm $^{-2}$ were fully amorphized. Two possible explanations account for the discrepancy between the SRIM and Raman results. First, the Raman laser's penetration depth is greater than the amorphous layer thickness created by 10 keV Ga ions, allowing undamaged regions beneath the amorphous layer to be detected, resulting in G peaks in the Raman spectra. Moreover, amorphization was observed after implantation with 20 and 30 keV at higher fluences due to the formation of thicker amorphous layers, which approach the Raman laser penetration depth in HOPG.

Second, the dpa required for amorphizing the HOPG samples in this study is significantly higher than that reported previously. Implantation at 20 keV with fluences of 2×10^{16} cm $^{-2}$ and 4×10^{16} cm $^{-2}$ produced amorphous layers of nearly identical thickness (see Table 1) but with varying maximum dpa, as predicted by SRIM. Nonetheless, Raman spectra indicated that only the samples implanted at the higher fluence of 4×10^{16} cm $^{-2}$ were completely amorphized. Consequently, the SRIM and Raman results suggest that achieving complete amorphization of our HOPG samples requires a dpa exceeding 35 dpa, significantly higher than the previously reported value of 0.20 dpa. This discrepancy may be attributed to the highly ordered structure of the HOPG samples used in this study, which necessitates higher fluences for complete damage (i.e., amorphization).

Data availability

The datasets used and/or analysed during the current study available from the corresponding author on reasonable request.

Received: 12 May 2025; Accepted: 16 September 2025

Published online: 18 November 2025

References

- Inagaki, M. *New Carbons-Control of Structure and Functions* (Elsevier, 2000).
- Guell, A. G., Tan, S. Y., Unwin, P. R. & Zhang, G. Electrochemistry at highly oriented pyrolytic graphite (HOPG): Toward a new perspective. *Electro. Carb. Elect.* **12**, 31–82 (2015).
- Ivekovic, D. et al. High-energy heavy ion irradiation of HOPG. *J. Nucl. Mater.* **578**, 154370 (2023).
- Guazzelli, M. A. et al. Effects of neutron radiation on the thermal conductivity of highly oriented pyrolytic graphite. *D. Rel. Mater.* **151**, 111803 (2025).
- Spemann, D., Han, K. H., Esquinazi, P., Hohne, R. & Butz, T. Ferromagnetic microstructures in highly oriented pyrolytic graphite created by high energy proton irradiation. *Nucl. Instrum. Methods Phys. Res. B.* **219**, 886–890 (2004).
- Koguchi, Y. et al. Modification of highly oriented pyrolytic graphite (HOPG) surfaces with highly charged ion (HCI) irradiation. *Nucl. Instrum. Methods Phys. Res. B.* **206**, 202–205 (2003).
- Hu, Z. et al. Effect of stress on irradiation responses of highly oriented pyrolytic graphite. *Materials* **15**, 3415 (2022).
- Konobeyev, A. Y., Fischer, U., Korovin, Y. A. & Simakov, S. P. Evaluation of effective threshold displacement energies and other data required for the calculation of advanced atomic displacement cross-sections. *Nucl. Energy Technol.* **3**, 169–175 (2017).
- Abe, H., Naramoto, H., Iwase, A. & Kinoshita, C. Effect of damage cascades on the irradiation-induced amorphization in graphite. *Nucl. Instrum. Methods Phys. Res. B.* **127**, 681–684 (1997).
- Harris, P. J. F. & Tsang, S. C. High-resolution electron microscopy studies of nongraphitizing carbons. *Philos. Mag. A Condens. Matter. Struct. Defects Mech. Prop.* **76**, 667–677 (1997).
- Niwase, K., Nakamura, K. G., Yokoo, M., Kondo, K. & Iwata, T. Pathway for the transformation from highly oriented pyrolytic graphite format into amorphous diamond. *Phys. Rev. Lett.* **102**, 116803 (2009).
- M.S. Dresselhaus, R. Kalish, *Implantation-Induced Modifications to Graphite*. In: *Ion Implantation in Diamond, Graphite and Related Materials*, Sprin. Ser. in Mat. Sci. 22 (2013).
- Li, Y. et al. A method to predict texture effect on ion beam channeling analysis of polycrystals and the application to study the mosaic spreading effect in highly oriented pyrolytic graphite. *J. Appl. Phys.* **131**, 22 (2022).
- Kangai, N., Tanabe, T. & Niwase, K. Damaging process of graphite and diamond studied by Auger electron spectroscopy and laser Raman spectroscopy. *J. Nucl. Mater.* **212**, 1234–1238 (1994).
- Matsunaga, A., Kinoshita, C., Nakai, K. & Tomokiyo, Y. Radiation-induced amorphization and swelling in ceramics. *J. Nucl. Mater.* **179**, 457–460 (1991).
- Kangai, N. & Tanabe, T. In situ AES study of damaging process of graphite surface under energetic ion bombardment. *J. Nucl. Mater.* **220**, 776–780 (1995).
- Alimov, V. K., Scherzer, B. M. U., Chernikov, V. N. & Ullmaier, H. Helium reemission desorption and microstructure evolution of graphites under helium ion implantation. *J. Appl. Phys.* **78**, 137–148 (1995).
- Chernikov, V. N., Kesternich, W. & Ullmaier, H. Radiation effects and gas cavities in pyrolytic graphite implanted with helium ions. *J. Nucl. Mater.* **227**, 157–169 (1996).
- Melinon, P. et al. Ion beam nanopatterning in graphite: Characterization of single extended defects. *Nanotechnol.* **19**, 235305 (2008).
- Tanabe, T. Radiation damage of graphite-degradation of material parameters and defect structures. *Phys. Scrip.* **64**, 7 (1996).
- Adejo, S. et al. Effects of implantation temperature and annealing on structural evolution and migration of Se into glassy carbon. *Solid State Sci.* **129**, 106914 (2022).

22. Jafer, T. A. O., Odutemowo, O. S., Abdelbagi, H. A. A., Thabethe, T. T. & Malherbe, J. B. The effect of ion implantation and annealing temperatures on the migration behavior of ruthenium in glassy carbon. *Nucl. Instrum. Methods Phys. Res. B* **557**, 16553 (2024).
23. Ni, Z., Wang, Y., Yu, T. & Shen, Z. Raman spectroscopy and imaging of graphene. *Nano Res.* **1**, 273–291 (2008).
24. K.J. Stevenson, *Review of Originpro 8.5*, J. Am. Chem. Soc. 133 (2011) 5621.
25. J. Ziegler, *SRIM 2012 computer code*, 2012. URL: www.srim.org.
26. Orlando, A. et al. A comprehensive review on Raman spectroscopy applications. *Chemosensors* **9**, 262 (2021).
27. Hossain, M. D., Zhang, Q., Cheng, T., Goddard, W. A. III. & Luo, Z. Graphitization of low-density amorphous carbon for electrocatalysis electrodes from ReaxFF reactive dynamics. *Carbon* **183**, 940–947 (2021).
28. Diaf, H. et al. Revisiting thin film of glassy carbon. *Phys. Rev. Mater.* **6**, 066002 (2020).
29. Bartali, R. et al. Interaction of the helium, hydrogen, air, argon, and nitrogen bubbles with graphite surface in water. *ACS Appl. Mater. Interfaces.* **9**, 17517–17525 (2017).
30. Melinon, P. et al. Ion beam nanopatterning in graphite: Characterization of single extended defects. *Nanotechnology* **19**, 235305 (2008).

Author contributions

T.A.O. Jafer: Writing—original draft, Methodology, Investigation, Conceptualization. H.A.A. Abdelbagi: Writing—original draft, Methodology, Investigation, Conceptualization. A. Sulyok: Writing—review & editing, Investigation. G.Z. Radnóczy: Writing—review & editing, Investigation. K. Tőkési: Writing—review & editing, Supervision, Methodology, Investigation, Funding acquisition, Conceptualization. J.B. Malherbe: Writing—review & editing, Supervision, Methodology, Investigation, Funding acquisition, Conceptualization.

Funding

This study was financially supported by the University of Pretoria which is gratefully acknowledged. We would like to thank Mr. R. Adam from the University of Pretoria for his assistance with Raman measurements. The work was also supported by the Bilateral relationships between South Africa and Hungary in science and technology (S&T) under the project number 2019-2.1.11-TÉT-202000123.

Declarations

Competing interests

The authors declare no competing interests.

Additional information

Correspondence and requests for materials should be addressed to K.T.

Reprints and permissions information is available at www.nature.com/reprints.

Publisher's note Springer Nature remains neutral with regard to jurisdictional claims in published maps and institutional affiliations.

Open Access This article is licensed under a Creative Commons Attribution-NonCommercial-NoDerivatives 4.0 International License, which permits any non-commercial use, sharing, distribution and reproduction in any medium or format, as long as you give appropriate credit to the original author(s) and the source, provide a link to the Creative Commons licence, and indicate if you modified the licensed material. You do not have permission under this licence to share adapted material derived from this article or parts of it. The images or other third party material in this article are included in the article's Creative Commons licence, unless indicated otherwise in a credit line to the material. If material is not included in the article's Creative Commons licence and your intended use is not permitted by statutory regulation or exceeds the permitted use, you will need to obtain permission directly from the copyright holder. To view a copy of this licence, visit <http://creativecommons.org/licenses/by-nc-nd/4.0/>.

© The Author(s) 2025